21st International Conference **ENGINEERING MECHANICS 2015**
Svratka, Czech Republic, May 11 –14, 2015
Full Text Paper **#180, pp. 3–11**

CFD Analysis of the Coolant Flow in Fuel Assembly of the VVER1000 Type Reactor

V. Heidler[1, a], J. Vimmr[2, b] and O. Bublík[3, c]

[1]Ing. Václav Heidler: Department of Mechanics, Faculty of Applied Sciences, University of West Bohemia, Univerzitni 8, 306 14 Pilsen, Czech Republic

[2]Assoc. Prof. Jan Vimmr, PhD.: Department of Mechanics, Faculty of Applied Sciences, University of West Bohemia, Univerzitni 8, 306 14 Pilsen, Czech Republic

[3]Ing.Ondřej Bublík, PhD.: Department of Mechanics, Faculty of Applied Sciences, University of West Bohemia, Univerzitni 8, 306 14 Pilsen, Czech Republic

[a]v.heidler@kme.zcu.cz, [b]jvimmr@kme.zcu.cz, [c]obublik@kme.zcu.cz

Keywords: Computational fluid dynamics, Lattice Boltzmann method, grid refinement, Grid-To-Rod fretting, Fuel assembly.

Abstract: The paper deals with the simulation of 3D coolant flow in a fuel assembly of the reactor VVER 1000 of the Temelín Nuclear Power Plant. Because of a very complex geometry and a large computational domain, it is a very computationally demanding task. With this in mind, some measure of simplification is inevitable. The lattice Boltzmann method was used for its simplicity and efficiency. The mathematical model of 3D coolant flow is solved using in-house software.

Introduction

Due to the transverse coolant flow in the core of a pressurized water reactor (PWR), fuel assemblies and their fuel rods are excited to oscillate. At beginning of life of the fuel assembly there is an interference fit between fuel rod and spacer grid, the springs of spacers are supporting the fuel rod under a certain preload. The preload of the springs decreases during the reactor operation due to the neutron irradiation. Due to this reduction or provided that there are some inaccuracies in manufacturing of fuel rods or grids, the spring force can decrease to zero, or rod to grid gap opening may appear [11]. Afterwards it is quite likely that the mechanical vibrations, whose amplitude is in the micrometer range cause excessive wear of their cladding in the areas of contact with the grids. In extreme cases, grid-to-rod fretting phenomena (GTRF) can, during the operation, results in breaking the first safety barrier with subsequent leakage of fissile products into the circulating primary coolant. In the nuclear power plants fretting wear of the cladding tube reduces fuel assembly service life and increases reactor operating costs. GTRF has been the major cause of fuel leakage in PWRs for the past ten years. The predictive simulations of this very complex phenomenon involve turbulence flow, structural dynamics, contacts and wear.

The aim of the present study is to simulate the unsteady turbulent coolant flow in the simplified part of fuel assembly using the lattice Boltzmann method (LBM). The results serves for understanding the complex fluid flow in PWR fuel assemblies and it is the first necessary step for describing Grid-To-Rod fretting phenomena.

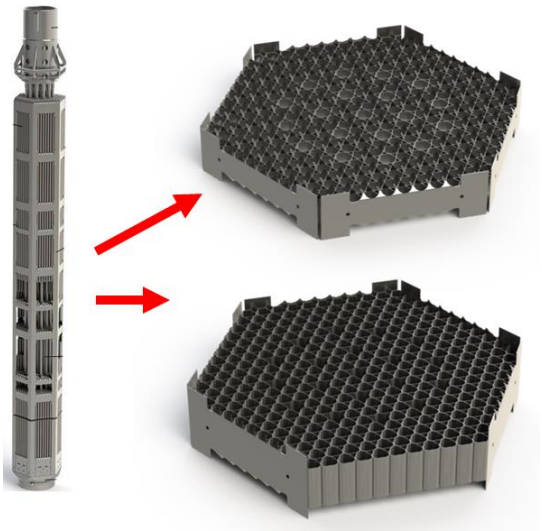

Fig. 1: VVER1000 fuel assembly with detail of mixing (the upper one) and spacer grid (the lower one).

Lattice Boltzmann method

In the recent past decades, the LBM has developed to a promising alternative approach to face problems in the field of CFD and has become an alternative to the conventional computational fluid dynamics methods for solving Navier-Stokes equations.

The lattice Boltzmann equation (LBE), the differential scheme of the LBM, is directly derived from celebrated Boltzmann equation (BE)

$$\frac{\partial f(t,\boldsymbol{x},\boldsymbol{\xi})}{\partial t} + \boldsymbol{\xi}\frac{\partial f(t,\boldsymbol{x},\boldsymbol{\xi})}{\partial \boldsymbol{x}} = \tilde{\Omega}(f), \tag{1}$$

where the $f(t,\boldsymbol{x},\boldsymbol{\xi})$ is the continuous particle distribution function (PDF), perform the probability of a particle to exist at location $\boldsymbol{x}$ at time t with velocity $\boldsymbol{\xi}$. The collision operator $\tilde{\Omega}(f)$ models the interaction of particles located at $\boldsymbol{x}$. Discretizing of BE in both time and velocity field, we obtain the LBE in the form

$$f_\alpha(t+\Delta t, \boldsymbol{x}+\boldsymbol{\xi}_\propto \Delta t) = f_\alpha(t,\boldsymbol{x}) + \Omega_\alpha, \tag{2}$$

where f_α, $\alpha = 1,2,\ldots Q$ are the discrete parts of distribution function corresponding to each microscopic velocity $\boldsymbol{\xi}_\propto$. The number Q of discrete microscopic velocities is related to the applied velocity model. We discuss the *D3Q19* model in this work [12], which is shown in Fig. 2. The collision operator Ω_α on the right-hand side of Eq. 2 perform the complex source term related to the particle interactions. One possible approximation is the multi-relaxation time scheme [4], which models the collision in the following way

$$\boldsymbol{\Omega} = \boldsymbol{M}^{-1}\boldsymbol{S}[(\boldsymbol{Mf}) - \boldsymbol{m}^{\boldsymbol{eq}}]. \tag{3}$$

Matrix $\boldsymbol{M}$ is the transformation matrix composed of the 19 orthogonal basis vectors. The moments of distribution functions $\boldsymbol{m} = \boldsymbol{Mf}$ are labeled as

$$\boldsymbol{m} = \left(\rho, e, \epsilon, j_x, q_x, j_y, q_y, j_z, q_z, 3p_{xx}, 3\pi_{xx}, p_{ww}, \pi_{ww}, p_{xy}, p_{yz}, p_{xz}, m_x, m_y, m_z\right). \tag{4}$$

The vector $\boldsymbol{m}^{eq}$ contains the equilibrium moments of PDFs given as

$$
\begin{aligned}
&m_0^{eq} = \delta\rho,\\
&m_1^{eq} = -11\delta\rho + \frac{19}{\rho_0}\boldsymbol{j}\cdot\boldsymbol{j},\\
&m_2^{eq} = \omega_\epsilon\delta\rho + \frac{\omega_{\epsilon j}}{\rho_0}\boldsymbol{j}\cdot\boldsymbol{j},\\
&m_{3,5,7}^{eq} = j_{x,y,z},\\
&m_{4,6,8}^{eq} = -\frac{2}{3}j_{x,y,z},\\
&m_9^{eq} = \frac{1}{\rho_0}(3j_x^2 - \boldsymbol{j}\cdot\boldsymbol{j}),\ m_{11}^{eq} = \frac{1}{\rho_0}\left(j_y^2 - j_z^2\right),\\
&m_{10}^{eq} = \omega_{xx}m_9^{eq},\ m_{12}^{eq} = \omega_{xx}m_{11}^{eq},\\
&m_{13}^{eq} = \frac{1}{\rho_0}j_xj_y,\ m_{14}^{eq} = \frac{1}{\rho_0}j_yj_z,\ m_{15}^{eq} = \frac{1}{\rho_0}j_zj_x,\\
&m_{16}^{eq} = m_{17}^{eq} = m_{18}^{eq} = 0.
\end{aligned}
\tag{5}
$$

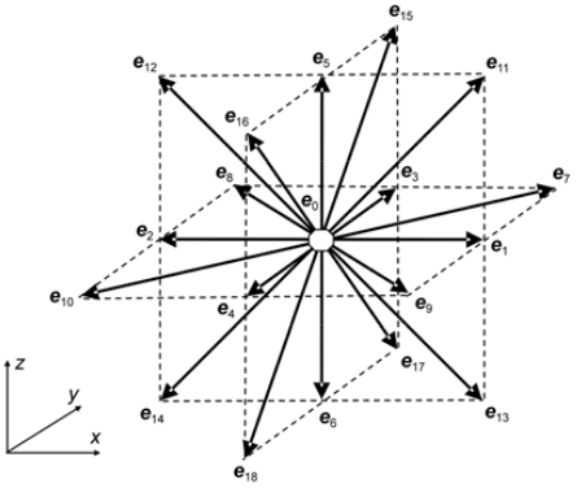

Fig. 2: D3Q19 lattice model.

The equilibria of the moments in Eq. 5 are functions of the conserved moments, which are mass density ($\rho = \rho_0 + \delta\rho$) and momentum ($j = \left(j_x, j_y, j_z\right) = \rho_0\boldsymbol{u}$). The density variation $\delta\rho$ instead of the total density is used to reduce the numerical effects due to round-off error [2,7]. The mean density in the system ρ_0 is usually set to 1. The parameters in the equilibria in Eq. 5 are chosen as follows to optimize the linear stability of the model ($\omega_\epsilon = \omega_{xx} = 0$ and $\omega_{\epsilon j} = -475/63$, see for details [4]).
The collision matrix $\boldsymbol{S}$ is the diagonal matrix containing collision parameters (the eigenvalues of the collision matrix $\boldsymbol{M}^{-1}\boldsymbol{S}\boldsymbol{M}$). The some recommended values can be found in [4].

Due to high Reynolds number (approximately 10^5), the flow inside the fuel assemblies is of turbulent nature. In this work we are using LES simulations model for capturing the deterministic unsteadiness of large eddy motions. In LES simulations, an additional viscosity, called the turbulent (or eddy) viscosity ν_t is introduced in order to model the turbulence. In the Smagorinsky model [7,8], the eddy viscosity is determined from the filtered strain rate tensor $S_{\propto\beta} = \left(\frac{\delta u_\beta}{\delta\propto} + \frac{\delta u_\propto}{\delta\beta}\right)/2$, a filtered length scale Δ and the Smagorinsky constant C_s

$$\nu_t = (C_s\Delta_x)^2\bar{S}, \quad \bar{S} := \sqrt{2S:S}. \tag{4}$$

In MRT collision operator model, $S_{\propto\beta}$ can be computed directly from non-equlibrium moments [9].

Mesh refinement

A significant drawback of LES method is the need for a fine grid spacing in the neighborhood of the wall. With this in mind we have implemented two type of grid refinement.

Hierarchically refined mesh with multiblock approach

This approach serves for local refining with respect to arbitrarily shaped objects. The whole domain is decomposed into the equally sized blocks. Some blocks, for example, which are near a boundary layer of wall surfaces, are then separated into eight new blocks with the same number of sites and half distance between them. The same process is repeated until the appropriate size between the sites is reached (Fig. 3).

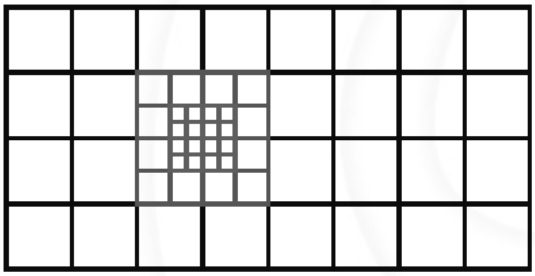

Fig. 3: 2D example of hierarchically refined mesh with multiblock approach.

With this approach, a communication and overlapping between the blocks with different level of refinement is needed (Fig. 4). The two-way coupling between a coarse and a fine grid involves two fundamental operations. When going from the fine to the coarse grid the amount of information must be reduced (filtering operations [1,10] on the set of sites $x_{f\to c}$ marked in Fig. 4), while we have to estimate the missing information when going from the coarse to the fine grid (cubic interpolation on the set of sites $x_{c\to f}$ marked in Fig. 4).

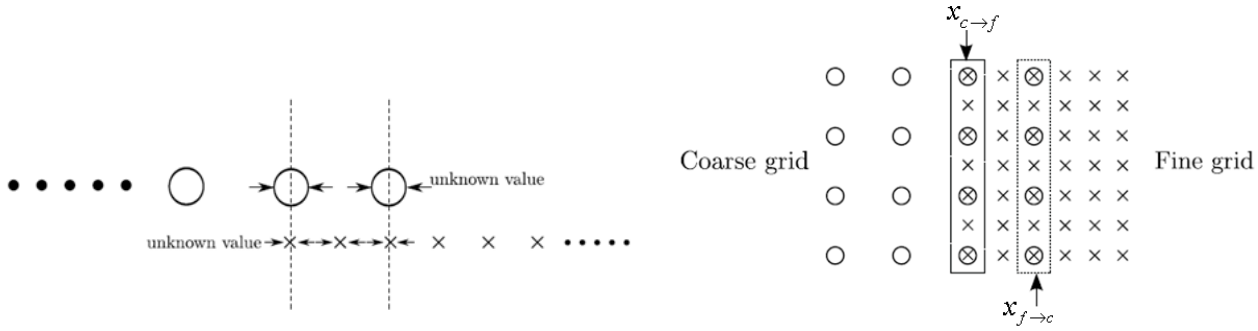

Fig. 4: Overlapping of the different grids.

Non-uniform Cartesian mesh

The vertical size of computational domain, owing to the quite long and very thin fuel rods, is much greater than the horizontal one. With this in mind, some algorithm for non-uniform Cartesian mesh (mesh lines are straight lines) is inevitable. To have an efficient LBM 3D solver we have applied the approach based on the one-dimensional interpolation via lagrange coefficients.

The principle of the method is, after the collision sub-process by the second-order local interpolation, to evaluate $g_\propto$ at the site $\boldsymbol{x} - \boldsymbol{e}_\propto \delta t$ („□" positions of 2D example in Fig. 5), which for non-uniform mesh may not be the mesh points. The streaming operation will be carried out from „□" to the mesh point „●" afterwards.

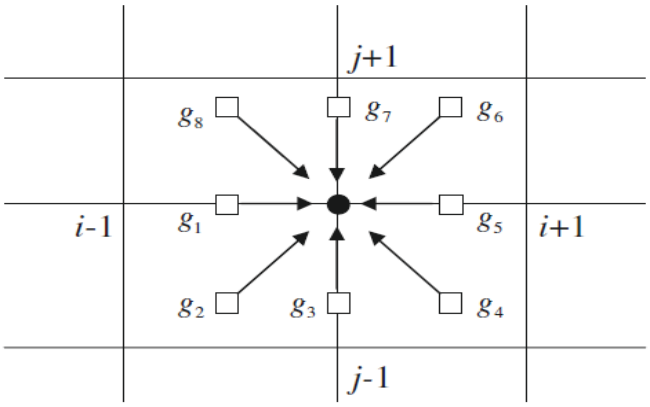

Fig. 5: 2D example of interpolation scheme.

Computational model

For the numerical simulations of coolant flow in fuel assembly we have restricted the geometry only to one fuel rods and its vicinity. For simplicity of the model we also contemplate only the grid containing mixing vanes (Fig. 1). The computational domain has size 22 x 25.4 x 57 [mm] and is illustrated in Fig. 6.

The parameters were determined to approximate the operating conditions in the reactor. Temperature 289 [°C] is the mean temperature at the outlet of the main circulation loops, and pressure 15.75 [MPa] is the pressure at the outlet of the core. The coolant PWR is water with 12.0 [g/kg] concentration of boric acid (H3BO3), which is neglected in the CFD simulation. Required properties (density, dynamic viscosity) are calculated with sub-program developed according to the latest international standard for water properties ($\rho = 749\ \left[\frac{kg}{m^3}\right], \mu = 9.3e^{-5}\ \left[\frac{Pa}{s}\right]$).

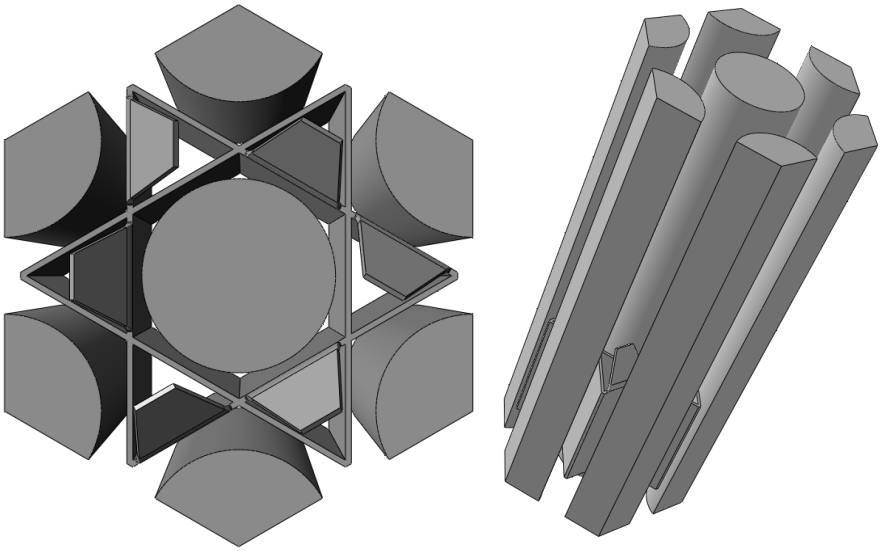

Fig. 6: Simplified geometry of part of fuel assembly.

The non-uniform hierarchically refined mesh contains 3 105 057 lattice sites and is shown in Fig. 7.

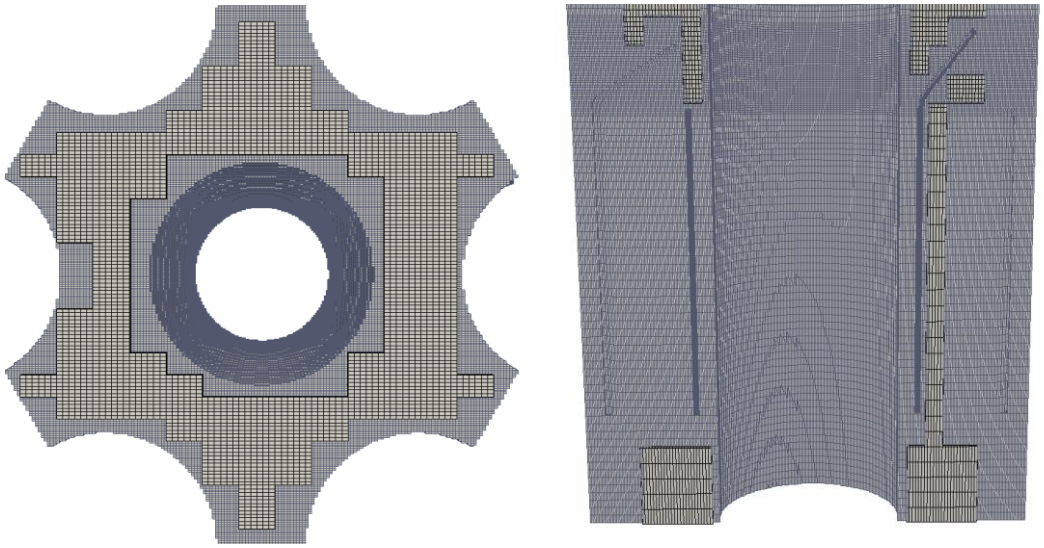

Fig. 7: Computational grid.

At the inlet the constant velocity profile ($u = 4\ \left[\frac{m}{s}\right]$) is prescribed. This value was chosen to represent some possible velocity inside the fuel assembly. At the outlet of the domain the zero

pressure gradient is considered. All of the solid surfaces are taken for no-slip walls. In LBM no-slip condition is typically represented by so called Bounce-Back scheme. It's mean that when the fluid particle reaches a boundary node, will be scatter back to the fluid along its incoming direction.

Numerical results

The transient simulation of 3D coolant flow was performed until the time 0.3 [s]. The Fig. 9,10 shows the contours of velocity magnitude at time 0.3 [s]. The positions of radial cross-section illustrated in Fig. 10 are highlighted in the Fig. 9 of axial cross-section.

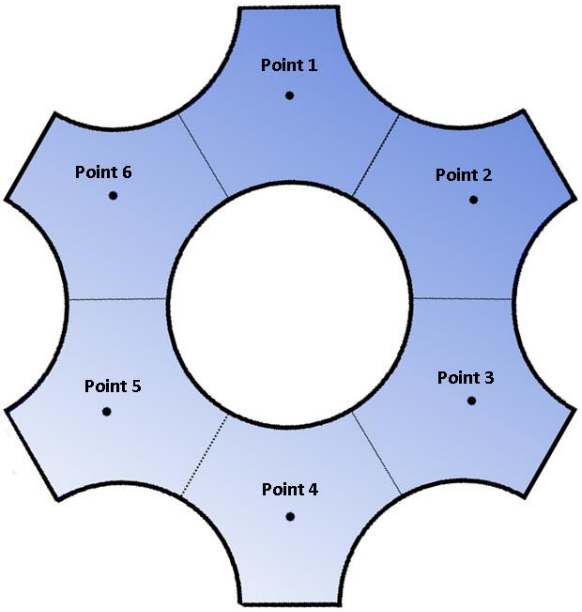

Fig. 8: Localization of checkpoints.

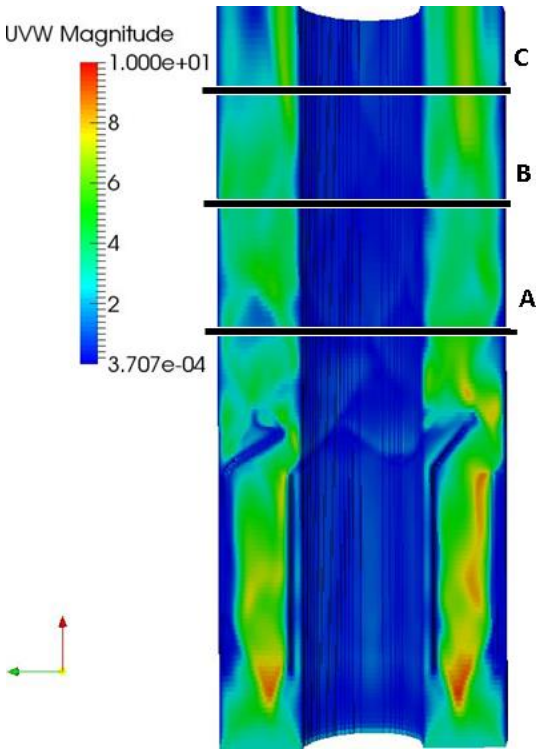

Fig. 9: Velocity contours at axial cross-section.

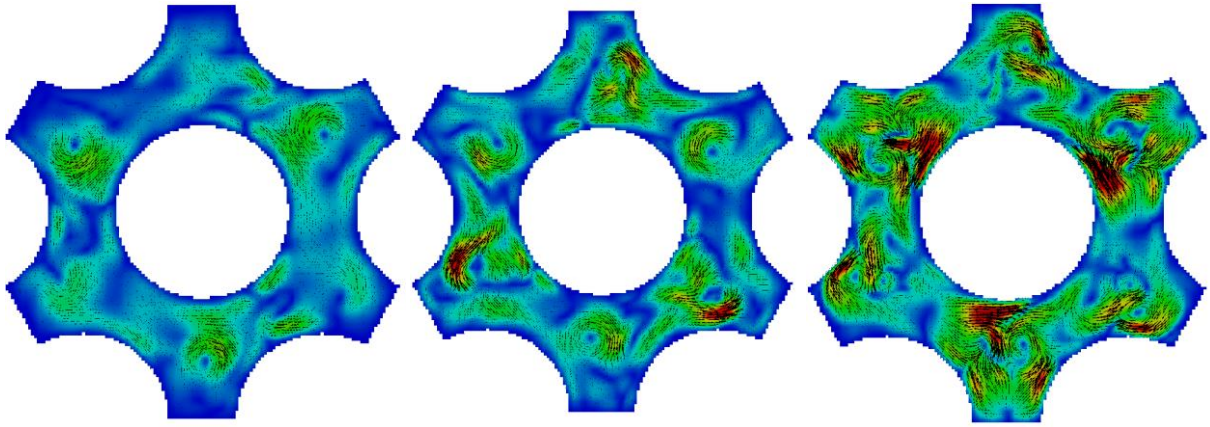

Fig. 10: Velocity contours at radial cross-section.

For evaluating of lateral flow intensity the time behavior of one radial velocity component is represented in graphs in Fig. 11÷13. The velocity component is plotted again the time in particular cross-section (Fig. 9) and in six selected checkpoints situated in the middle of subchannels (see Fig. 8). The results obtained with the lattice Boltzmann method are in a relatively good qualitative agreement with what we would expect.

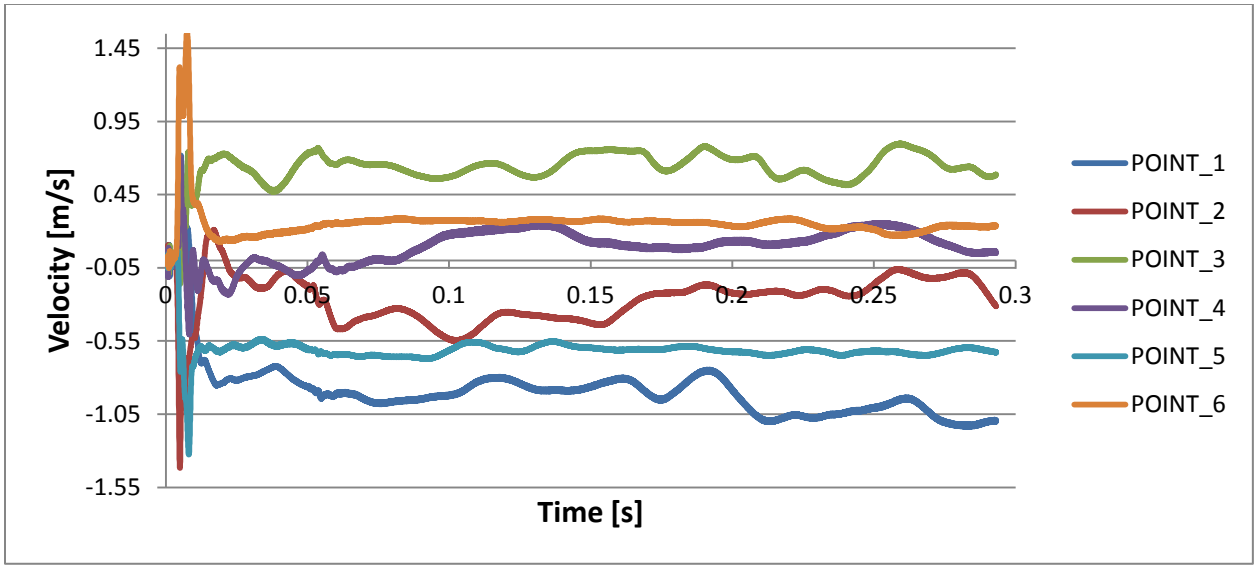

Fig. 11: Radial component of velocity plotted again the simulation time at cross-section A.

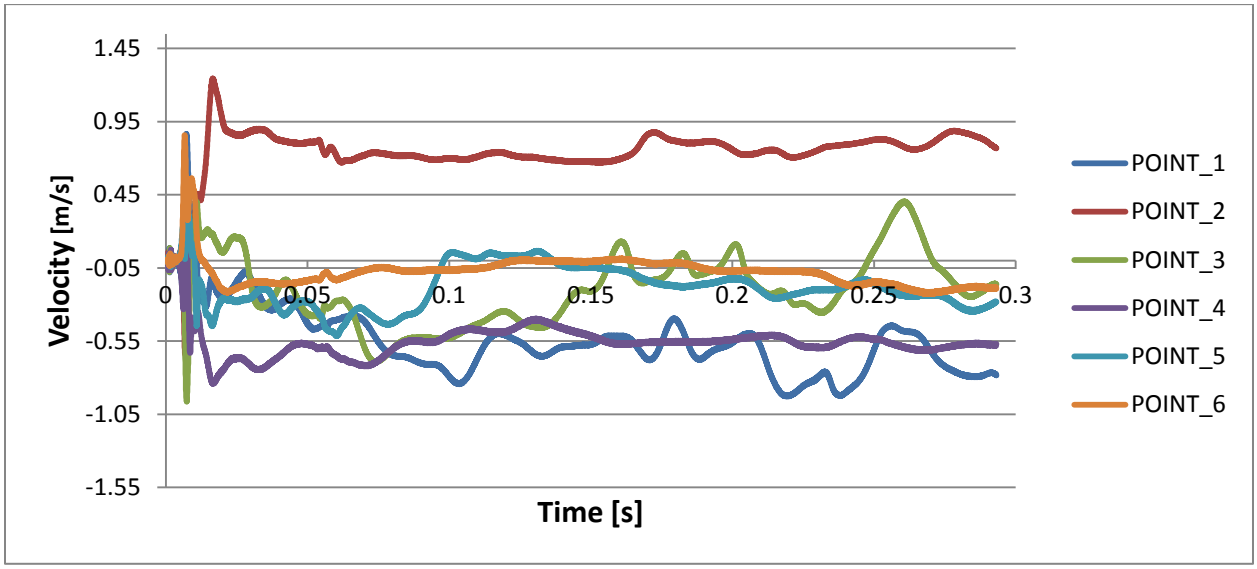

Fig. 12: Radial component of velocity plotted again the simulation time at cross-section B.

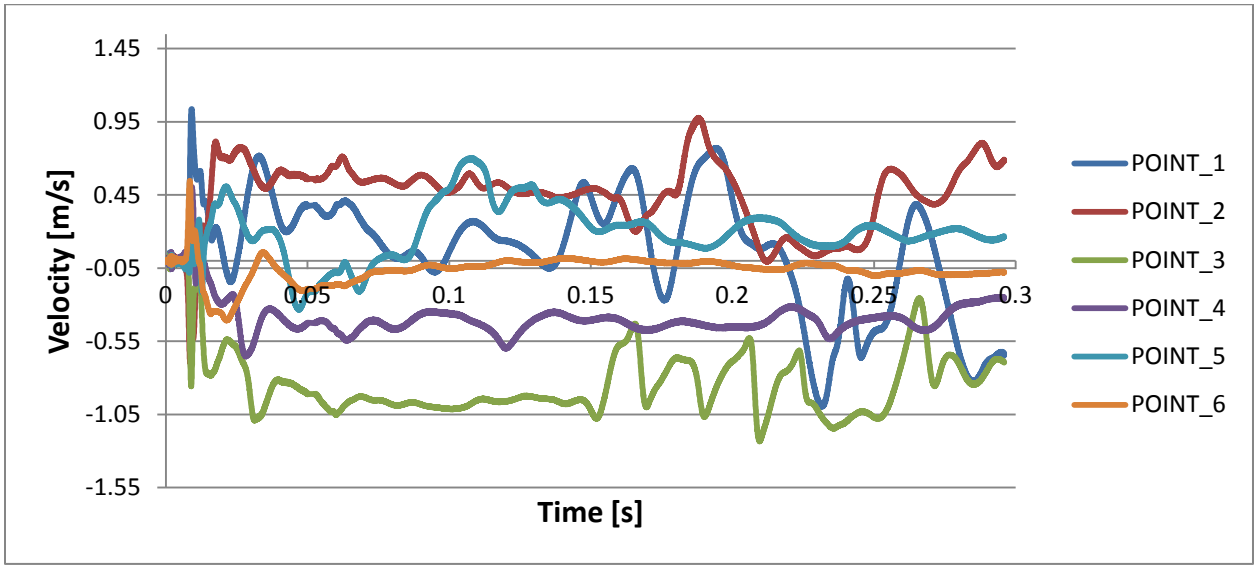

Fig. 13: Radial component of velocity plotted again the simulation time at cross-section C.

Summary

We have implemented the lattice Boltzmann method for solving large-eddy simulation of the coolant flow in the fuel assembly using multiple-relaxation-time model, recursively refined meshes using hierarchical block structured grids, non-uniform grid based on the one-dimensional interpolation via lagrange coefficients and parallelization using Coarray Fortran. Main goal is to evaluate the lateral flow intensity and understand the fluid dynamics for the flow-induced vibration problem leading to GTRF. We found that the lattice Boltzmann method represents an applicable instrument to this type of large and complex flow.

Next task is to add energy equation into our in-house software and consequently the buoyancy force. Some emphasis will be also put on calculation the bigger domain with more than one mixing grid and for longer simulation time.

Acknowledgement

This study was supported by the internal student grant project SGS-2013-036 of the University of West Bohemia.

References

[1] L. Sandoval, D.Walter, Revisiting grid refinement algorithms for the lattice Boltzmann method, Thèse de doctorat, Univ. Genève, 2012, no. Sc. 4520.

[2] P.A. Skordos, Initial and boundary conditions for the lattice Boltzmann method, Phys.Rev. E 48:4823-4842, 1993.

[3] J. Tölke, M. Krafczyk, M. Schulz, E. Rank, Lattice Boltzmann simulations of binary fluid flow through porous media. Philos Trans Roy. Soc. Lond. A 2002; 360(1792):535–45.

[4] D. d'Humie`res, I. Ginzburg, M. Krafczyk, P. Lallemand, L-S. Luo, Multiple-relaxation-time lattice Boltzmann models in three dimensions, Philos. Trans. Roy. Soc. Lond. A 2002; 360:437–51.

[5] L-S. Luo, Unified theory of the lattice Boltzmann models for nonideal Gases, Phys. Rev. Lett. 1998;81(8):1618–21.

[6] O. Filippova, D. Hänel, Boundary-fitting and local grid refinement for LBGK models. Int. J. Mod. Phys. C 1998;8:1271.

[7] S.B. Pope, Turbulent flows. Cambridge: Cambridge University Press; 2000.

[8] J. Smagorinsky, General circulation experiments with the primitive equations: I. The basic equations. Mon Weather Rev 1963;91:99–164.

[9] H. Yu., L-S. Luo, LES of turbulent square jet flow using an MRT lattice Boltzmann model, Comput. Fluids 35(8), 957-965 (2006).

[10] Ricot D., Marié S., Sagaut P., Bailly C., Lattice Boltzmann method with selective viskosity filter, J.Comp. Phys., 228 (2009), pp. 4478-4490.

[11] A. Billerey, Evolution of Fuel Rod Support under Irradiation – Impact on the Mechanical Behaviour of Fuel Assemblies, Structural behaviour of fuel assemblies for water cooled reactors, IAEA-TECDOC-1454, pp.101-111, Vienna, 2005

[12] Qian.,Y.H., D'Humie`res, D., Lallemand, P., Lattice BGK Models for Navier-Stokes Equation, EPL (Europhysics Letters), 17(6):479, 1992.